International Journal of Robotics and Control Systems
Vol. 5, No. 2, 2025, pp. 748-762
ISSN 2775-2658
http://pubs2.ascee.org/index.php/ijrcs

Enhancing the Performance of Grid-Tied Renewable Power Systems Using an Optimized PI Controller for STATCOM

Mansour Aljohani [a,1,*]

[a] Yanbu Industrial College, Yanbu Al Sinaiyah, 46452, Saudi Arabia
[1] aljohanimansour75@gmail.com
* Corresponding Author

ARTICLE INFO

Article history
Received November 06, 2024
Revised February 03, 2025
Accepted February 13, 2025

Keywords
Elephant Herding Optimization (EHO);
Photovoltaic (PV) Systems;
Static Synchronous Compensator (STATCOM);
Sustainable Energy;
Wind Energy

ABSTRACT

Integrating electrical networks with renewable energy sources in hybrid systems may effectively meet increasing power demands while reducing reliance on traditional energy sources. Wind gusts in wind energy conversion systems (WECSs), along with variations in temperature and irradiance in photovoltaic (PV) systems, render these systems vulnerable. Three-phase faults at the point of common coupling (PCC) can disconnect renewable energy sources (RESs) from the grid, threatening system stability. This study enhances a hybrid PV-WECS system through the implementation of a static synchronous compensator (STATCOM) to mitigate wind gust effects and maintain RES connectivity during three-phase faults at the point of common coupling (PCC). STATCOM manages reactive power exchange between renewable energy sources and the grid through two PI controllers. The gains of the PI controller are optimized through elephant herding optimization (EHO), demonstrating superior performance compared to particle swarm optimization (PSO) in terms of PCC voltage stability and system efficiency. In three-phase faults, the EHO demonstrates superior performance over the PSO, achieving a PCC voltage of 0.7 in contrast to 0.37, thereby maintaining voltage levels within acceptable limits in the connecting zone according to grid codes. The EHO-optimized PI controllers for the STATCOM successfully reduce the SRG current during this fault, decreasing it from 155 (with PSO) to 111 (with EHO). Under wind gust conditions, the power profile obtained from the SRG is markedly enhanced when employing EHO in comparison to PSO.

1. Introduction

Integrating renewable energy sources (RESs) into electrical systems has become crucial to meet escalating energy consumption and mitigate fossil fuel emissions. Common RESs include wind, photovoltaic (PV), fuel cells, and biomass [1]-[4], with wind and PV the most widely deployed [5]. Global installed PV capacity now stands at around 1185 GW—over 6% of worldwide electricity consumption—rising from ~3% in 2019 [6]. Concurrently, global wind power capacity reached approximately 1021 GW in 2023 [7]. Hybridization efforts for various renewables aim to efficiently generate clean and economical power [8]-[10].

WECSs and PV-based hybrid power systems often do not supply sufficient reactive power during faults, causing voltage fluctuations at the RES–grid point of common coupling (PCC). These fluctuations can degrade system stability, power factor, and overall power quality. When reactive power is insufficient, voltage swings can escalate to unsafe levels. If not properly managed, RESs may disconnect from the grid to comply with regulations. Reactive power demands are met using flexible alternating current transmission systems (FACTS) [11], [12], which include series and shunt compensators or combined devices.

Series devices—often called dynamic voltage restorers (DVRs)—offer reactive power support to hybrid renewables, while shunt compensators such as static var compensators (SVCs), static synchronous compensators (STATCOMs), and superconductors also maintain voltage stability [13], [14]. Compound-type unified power flow controllers (UPFCs) have been applied to bolster grid connectivity for diverse RESs [15]. Multiple FACTS devices in series or shunt modes address sags, swells, and harmonics that can threaten grid stability [16]-[22]. As grids become more interconnected, advanced devices like DVRs, STATCOMs, and superconductors mitigate power-quality (PQ) issues [23]. Regulatory standards and customer expectations drive the adoption of sophisticated devices, particularly STATCOMs, to ensure uninterrupted high-quality supply.

Proportional–integral (PI) controllers remain prevalent thanks to simplicity and user-friendliness, enhancing performance in fuel cells, PV systems, and wind turbines [24]. However, inaccurate PI tuning can undermine system objectives. Hybrid systems, featuring nonlinear components such as converters and inverters, complicate PI parameterization under linear control methods. Consequently, conventional optimization methods have emerged to fine-tune PI controllers in these environments [25].

Among the most effective optimizers for PI gains is the genetic algorithm (GA) [26]. Contemporary methods include follower pollination and harmony search, while particle swarm optimization (PSO) also optimizes PI gains for inverters connecting fuel cells to the grid. WECS typically employ switched reluctance generators (SRGs), self-excited induction generators (SEIGs), or doubly-fed induction generators (DFIGs) [27]-[29]. Although DFIGs can tolerate wind velocity variations, slip rings often need maintenance. SRGs, despite lower maintenance requirements and robustness, still require external reactive support.

Elephant herding optimization (EHO) has proven successful for PV and WECS applications, particularly in refining proportional–integral–derivative (PID) tuning for frequency regulation [30]. Compared with PSO and teaching–learning-based methods, EHO yields efficient low-voltage ride-through in grid-connected wind generation. It can also optimally calibrate SRG–WECS off-delay angles for improved performance [31]. In parallel, whale optimization algorithm (WOA) sometimes surpasses PSO and cuckoo search (CSO).

STATCOM is a widely adopted FACTS device delivering reactive power compensation, voltage control, and dynamic stability [32]. Designing and controlling STATCOM for RES integration remains a challenge due to the nonlinear nature of these systems [33], [34]. Researchers have proposed methods such as GA, artificial neural networks (ANN), and adaptive-network-based fuzzy inference systems (ANFIS) to update the PI gains [35], [36]. WOA has also seen varied usage [37]. These optimization algorithms typically run offline to determine best-fit PI controller parameters.

EHO, a more recent approach [38], mimics elephant herding behavior to explore solution spaces under uncertain conditions effectively. While highly intricate problems can challenge EHO's search diversity, it remains robust for many applications. This work presents two optimized PI controllers for STATCOM, enabling integration of both WECS–SRG and PV. By adjusting reactive power flow between the system and STATCOM at PCC, voltage stability is improved and fault ride-through (FRT) is maintained. EHO mitigates the limitations of conventional PI optimization in grid-connected renewable systems, with PSO serving as a benchmark for performance comparisons.

This study examines the enhancement of grid integration for PV and WECS-based SRG through the incorporation of a STATCOM. The STATCOM is regulated through two PI controllers that have been optimized using the EHO algorithm. The proposed EHO-PI-STATCOM's effectiveness in improving the hybrid system is evaluated using two test cases. The initial case examines a three-phase

Vol. 5, No. 2, 2025, pp. 748-762

fault at the PCC to assess the connection stability of PV systems and WECS to the grid during the fault, following Spain's grid code. The second case assesses the improvement of the WECS power profile in response to wind gusts. The performance of the EHO-based optimization for the PI-STATCOM controller is compared with the PSO optimization technique.

2. System Under Investigation

The system under investigation consists of two RESs: WECS-SRG and PV, where the used SRG is a four-pole 8/6 type. The two RESs are connected to the system through a bus at PCC. Two transformers and two transmission lines connect the grid to this shared connector bus. Fig. 1 illustrates the connection between PCC and STATCOM, which is implemented to enhance the system performance. The Voltage Source Converter (VSC)-STATCOM type is utilized in this work. WECS-SRG has a power rating of 24.8 kW. The PV system has a capacity of 150 kW and consists of 100 strings, with each string comprising five modules connected in series [39]. This PV system incorporates the maximum power point tracking (MPPT) technique to optimize its energy production under different weather conditions. Here the used MPPT is the conventional incremental conductance. The detailed information about the system can be referred to Appendix. Each source (PV and SRG) is linked to PCC via the DC-DC converter and DC-AC inverter.

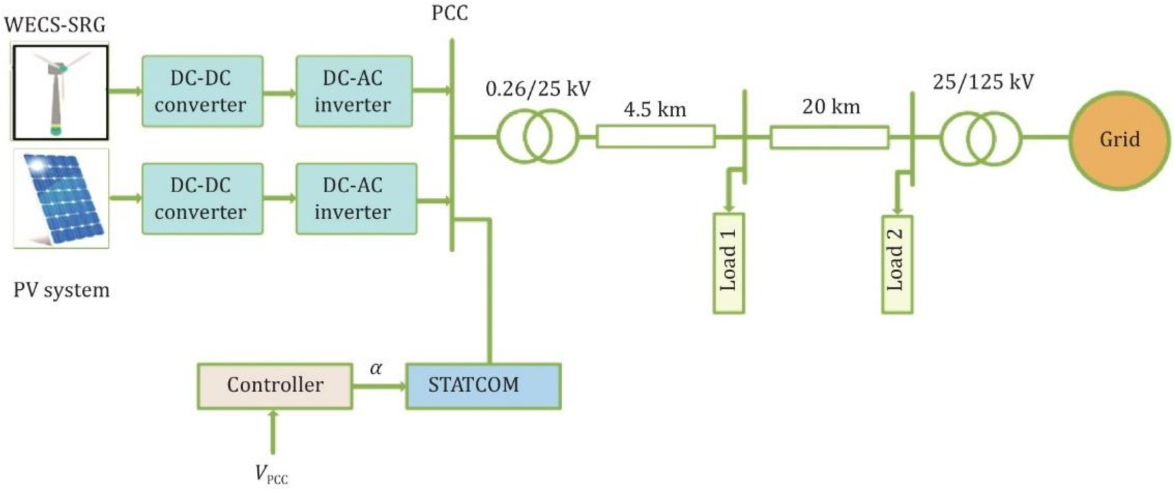

Fig. 1. System under investigation

3. System Modeling

3.1. Switched Reluctance Generator (SRG)

Switched reluctance generators (SRGs) exhibit several merits for WECS applications, such as mechanical robustness, simple design, high efficiency, broad operational speed range, and resilience to certain fault conditions. The stator windings use concentrated coils in a relatively simple arrangement. In the standard configuration, opposing stator windings connect in series to produce a two-pole field pattern. With no magnets on the rotor, windage decreases and inertia remains low. Owing to its doubly salient structure—salient stator and rotor poles—an asymmetric bridge converter excites the SRG. This study employs a four-phase, 8/6 SRG [30]. The linkage flux is defined by:

$$\lambda(t) = \int_0^t \left(V_{SRG} - i_s R_{s_{SRG}}\right) dt \tag{1}$$

where V_{SRG} is terminal voltage, i_s is the phase current, and $R_{s_{SRG}}$ is stator resistance.

The four SRG phases are excited via an asymmetric converter, allowing independent regulation of each phase current. Rotor position detection enables precise control of turn-on and turn-off angles for each phase. A four-channel hysteresis controller manages the stator phase currents. Magnetic flux linkage is computed by integrating the difference between input voltage and the drop across $R_{s_{SRG}}$.

The total SRG torque equals the sum of individual phase torques:

$$T_e = \sum_{j=1}^{N_{s_{SRG}}} T_j\,(\theta, i_s) \tag{2}$$

where $N_{s_{SRG}}$ is the number of phases and θ is the phase angle of the terminal voltage.

The average electrical power output is:

$$P_{out} = \frac{1}{T_G} \sum_{j=1}^{N_{s_{SRG}}} \int_0^T v_j\; i_{s_j}\, dt \tag{3}$$

Here, T_G denotes each phase conduction period; v_j and i_{s_j} are the voltage and current of phase j. Comprehensive SRG modeling details can be found in [20] and [27].

3.2. PV System

Photovoltaic (PV) systems offer notable cost advantages over other renewables. One common model uses a p–n diode and parallel current source [40], establishing a current–voltage (I–V) profile for the PV array. Fig. 2 depicts the PV module's equivalent circuit [31], where the output current is I and the output voltage is V, [45].

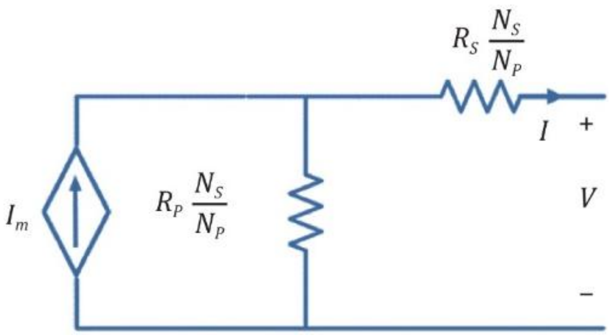

Fig. 2. Equivalent circuit of the PV module

The I–V characteristic is:

$$I_0 = \frac{I_{scn} + K_i \Delta T}{\exp\left(\frac{V_{ocn} + nK_v \Delta T}{aV_t}\right) - 1} \tag{4}$$

$$I_{pv} = \left(I_{pvn} + K_i \Delta T\right)\frac{G}{G_n}, \tag{5}$$

$$I_m = I_{pv}N_p - I_0 N_p \left[\exp\left(\frac{V + R_s\left(\frac{N_s}{N_p}\right) I}{V_t\, a\, N_s}\right) - 1\right] \tag{6}$$

where I_{pv}, V are the PV output current and voltage, I_{pvn} is photocurrent, I_0 is reverse saturation current, I_m is module current, N_p is parallel cell count, N_s is series cell count, n is diode ideality factor,

Vol. 5, No. 2, 2025, pp. 748-762

K_i, K_v are temperature coefficients, and ΔT is the temperature difference from nominal. V_{ocn} is the open-circuit voltage, G is instantaneous irradiance, and G_n is irradiance at nominal conditions. The thermal voltage V_t is:

$$V_t = \frac{N_s kT}{q} \tag{7}$$

where k is Boltzmann's constant, T is the absolute temperature, and q is electron charge [32], [33]. A conventional incremental conductance (INC)- MPPT algorithm is employed for the KC200GT module [30], [31].

3.3. STATCOM Modeling

Appendix Section 2 contains the general mathematical model for STATCOM, expressed via active power, reactive power, and STATCOM output voltage.

3.4. STATCOM Operation and Control

A STATCOM is powered through the PCC voltage, producing capacitive or inductive current. Fig. 3 illustrates the STATCOM system, including the coupling transformer linking the voltage source inverter (VSI) to the power network at the PCC, along with a DC capacitor for energy storage. The VSI generates a voltage with adjustable amplitude and synchronous frequency. Comparing the PCC voltage to the reference (1 p.u. at 0.26 kV) allows STATCOM to operate in capacitive or inductive modes. During undervoltage, STATCOM delivers a leading current (capacitive mode); in overvoltage scenarios, it draws current (inductive mode). Failure to adjust the PCC voltage results in zero power transfer. By injecting current to support PCC voltage during faults, STATCOM augments the dynamic stability of the hybrid power system [44].

Two PI controllers regulate the STATCOM to offset voltage variations. Here, EHO optimizes the PI parameters by minimizing the integral of the squared error (ISE) between the reference and PCC voltages [41], [42]. Controller 1 updates the quadrature-axis current ($I_{q_{ref}}$), based on the measured–reference voltage mismatch, while Controller 2 regulates the PCC terminal voltage angle (θ).

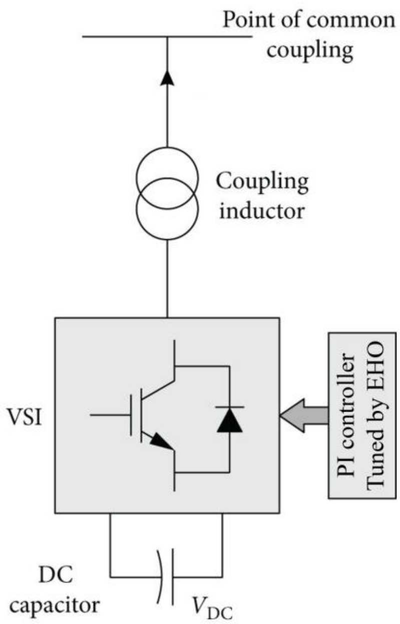

Fig. 3. STATCOM circuit representation

In this study, the three-level STATCOM inverter employs sinusoidal pulse width modulation (SPWM). The inverter output voltage phase angle controls the power flow into the grid [22]. EHO optimizes the PI controller parameters driving the STATCOM, while PSO serves as a comparative benchmark.

3.5. PSO for Tuning PI Control Parameters

Particle swarm optimization (PSO) is used to determine optimal PI gains for controlling reactive power flow between STATCOM and RES. Two PI controllers (each with a proportional and integral gain) manage the STATCOM. PSO updates controller parameters to minimize an objective function J. Iteratively, each particle's position and velocity are refined until the best global solution emerges [32].

3.6. Elephant Herding Optimization (EHO)

PI controller parameters significantly influence system performance, particularly for nonlinear RESs. Classic tuning approaches may be insufficient. EHO is a modern algorithm well-suited for PV and other applications. In this paper, EHO reduces the integral of squared error between the reference voltage ($V_{ref} = 22$ V) and actual DC voltage (V_{DC}):

$$J = \min \int \left(V_{ref} - V_{DC}\right)^2 dt \tag{8}$$

Drawing on natural elephant herd behavior, EHO partitions populations into subgroups (clans), updates positions based on a matriarch's leadership, and disrupts local minima through worst-position transformations [46]-[50]. Initialization sets EHO parameters, population size, maximum iterations, and potential solutions. Each elephant's position encodes four PI controller parameters, and the best solutions are updated dynamically until termination. EHO is mainly based on elephant herding behavior. Initialization sets EHO parameters, population size, maximum iterations, and potential solutions. Each elephant's position encodes four PI controller parameters, and the best solutions are updated dynamically until termination. For the detailed mathematical formulations of EHO ((9)–(12)), please refer to Appendix A. Fig. 4 depicts the EHO flow chart for STATCOM PI controller tuning.

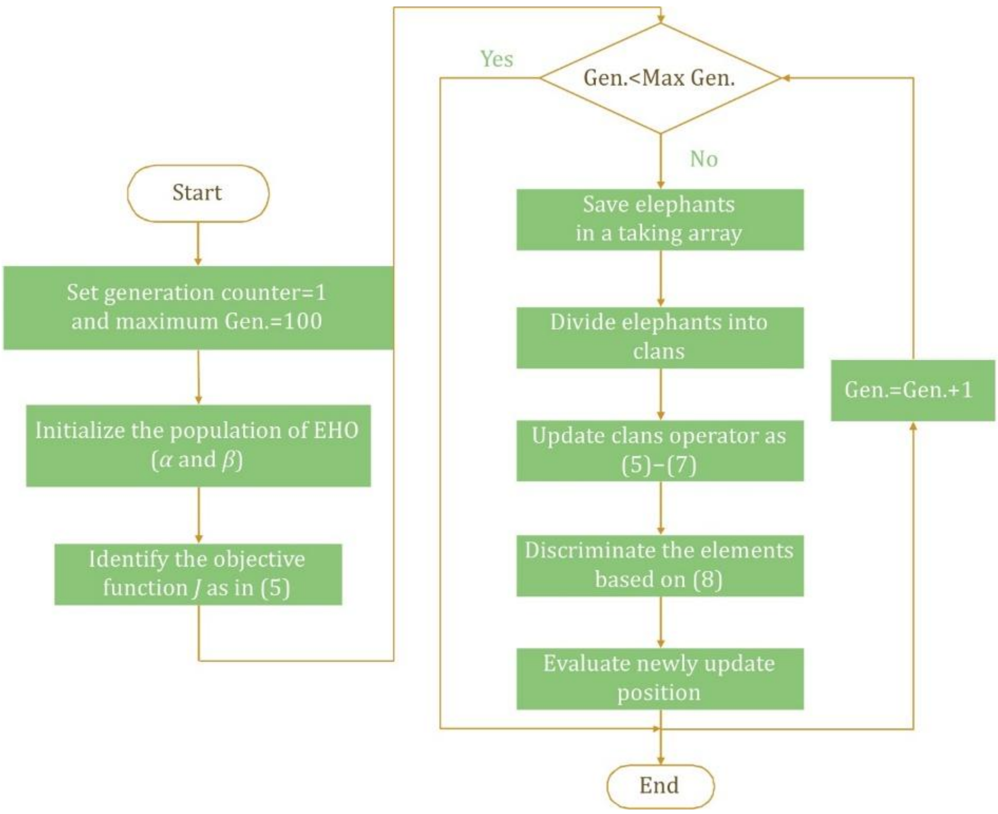

Fig. 4. Flow chart of the EHO method for optimizing the PI controller parameters

4. Results and Discussion

MATLAB/Simulink is used to simulate a grid-tied hybrid system (WECS–SRG + PV) with a controlled STATCOM. The system is evaluated under both three-phase faults and wind gust conditions, demonstrating reactive power management. In our experiments, both elephant herding optimization (EHO) and particle swarm optimization (PSO) are used to set the PI controller parameters for comparison [32], [43].

4.1. Three-Phase Fault

A three-phase fault (line-to-ground) is induced at the PCC from 2.00 s to 2.25 s, with a 48 kV STATCOM rating [14]. Fig. 5 illustrates the convergence of the objective function J. EHO outperforms PSO by achieving a minimum value of 0.25 against PSO's 0.36.

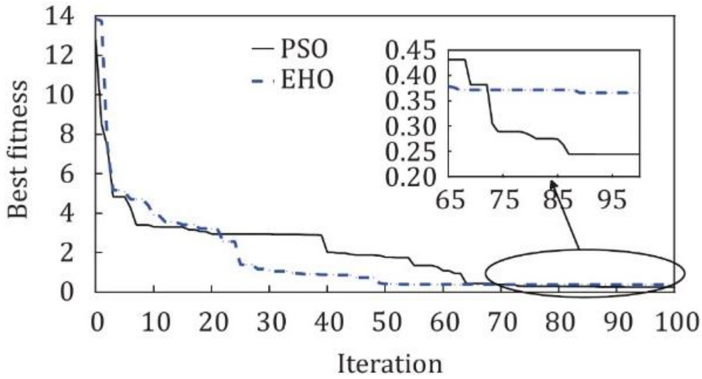

Fig. 5. PSO and EHO-based convergence of the objection function J

If PCC voltage deviates from accepted thresholds (per Spanish/US grid codes), RESs disconnect. Reconnection is complex. A well-tuned STATCOM boosts PCC voltage during faults. Using EHO yields minimum PCC voltages of 0.37 pu, compared with 0.59 pu from PSO, and exhibits lower overshoot (Fig. 6). Thus, EHO outperforms PSO.

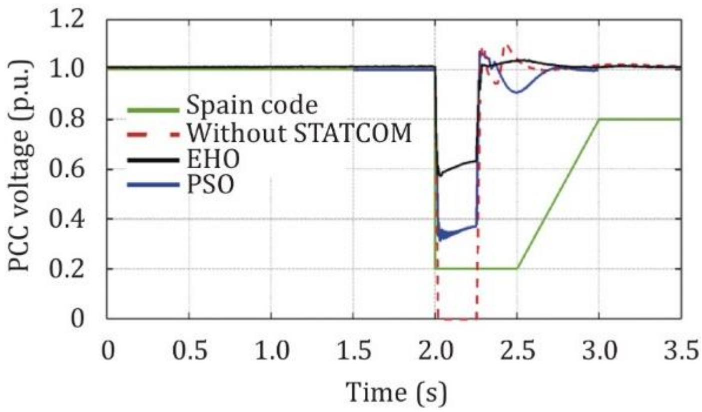

Fig. 6. PCC voltage with and without STATCOM during 3-phase fault

Because the STATCOM upholds the PCC voltage, the RESs endure short-circuit events without disconnecting. In the absence of STATCOM, the PCC current spikes to 1.43 pu, triggering overcurrent protection and disconnecting the RES. With STATCOM in place, PCC current only slightly increases (0.74 pu for PSO, 0.72 pu for EHO), as shown in Fig. 7.

4.1.1. SRG Performance

Post-fault clearance at 2.25 s sees SRG output power surge to 28 kW, which cannot revert to the steady-state value (25 kW) without STATCOM. With STATCOM support, the SRG power recovers to 25 kW (Fig. 8 a), and its current stabilizes near 155 A vs. 111 A otherwise (Fig. 8 b). Without STATCOM, overcurrent protection would disconnect the WECS entirely.

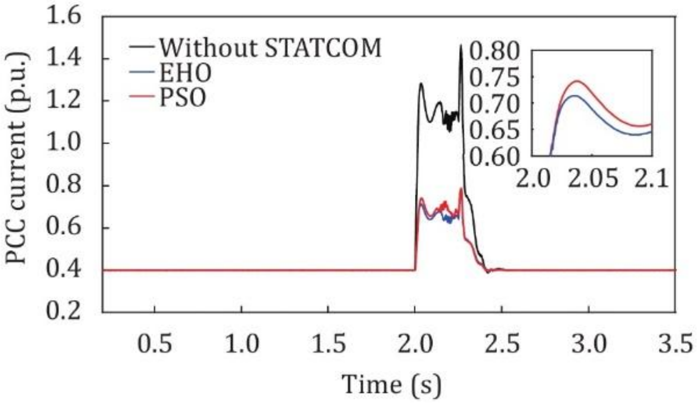

Fig. 7. PCC current with and without STATCOM during 3-phase fault

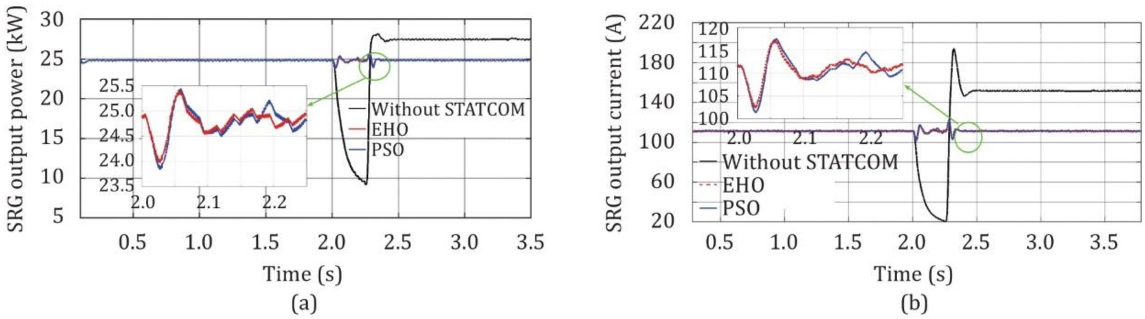

Fig. 8. SRG performance during 3-phase fault: (a) output power and (b) output current

4.1.2. PV Performance

Fig. 9 shows the PV system under three-phase faults. With MPPT, the PV adjusts operating voltage and current. Short-circuiting at the PCC causes transient voltage drops, but MPPT lowers the current to prevent overheating. As a result, the PV module rapidly returns to near-maximum power after fault clearance.

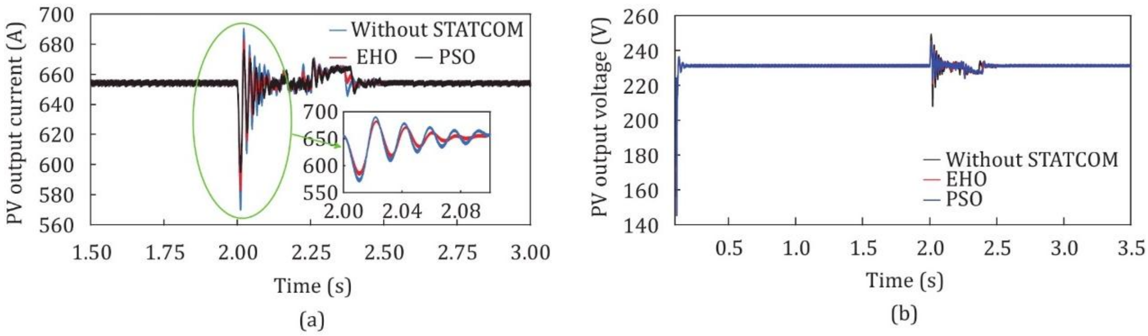

Fig. 9. PV performance during 3-phase fault: (a) output current and (b) output voltage

4.2. Wind Gust

A wind gust causes yet another disruption in the system by affecting the voltage profile at PCC and the SRG voltage. In this work, the wind gust is simulated by applying random wind speed variations to WECS between 2 m/s and 15 m/s, as shown in Fig. 10 (a). Without STATCOM, the PCC voltage varies around the rated value, with increased harmonics and distortions caused by wind gusts. The increased voltage at PCC is larger than that with STATCOM, as shown in Fig. 10 (b). As for the case with STATCOM, it is obvious that this value is lower when EHO is applied compared with that of PSO. STATCOMs are used to control voltage levels in the power system via providing reactive power assistance. It can stabilize the voltage in the presence of wind gusts, which results in rapid changes in the power output from WECS.

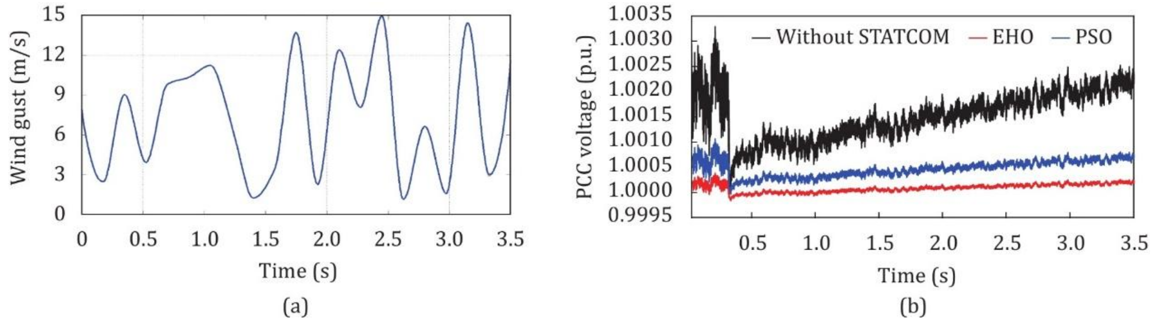

Fig. 10. Investigation on wind gust: (a) simulated wind gust and (b) PCC voltage variation during wind gust

5. Summary and Discussions

Similar studies [14] report minimum PCC voltages around 0.40 p.u., highlighting that our EHO-based method achieves competitive—if not superior—FRT performance. As shown in Table 1. The improved FRT is attributed to the reactive power injection by STATCOM, which swiftly counters voltage sags during faults.

Table 1. Comparison with prior work

Metric	Result		
	EHO-based STATCOM	**PSO-based STATCOM**	**WOA-based STATCOM [14]**
Minimum PCC Voltage (p.u.)	0.37	0.59	0.35
Convergence Objective (J)	0.25	0.36	0.29
Maximum PCC Current (p.u.)	0.72	0.74	0.73

The EHO method demonstrates enhanced efficacy relative to PSO by achieving faster convergence and improved fault ride-through (FRT) performance, as evidenced by reduced PCC voltage fluctuations and minimized current overshoots. Compared to previous studies, the EHO-based approach delivers superior performance metrics, highlighting its effectiveness in managing fault conditions and its potential applicability in real-world scenarios. A critical factor in this achievement is the STATCOM's ability to inject reactive power during both fault and wind gust events, which is essential for maintaining grid voltage stability.

However, this research also recognizes significant limitations. The simulation relies on a simplified grid model and assumes specific grid code parameters, which may not fully capture the complexities of actual power systems. Furthermore, although the simulation results are promising, the system's performance under more complex grid conditions and potential hardware imperfections has yet to be evaluated. Future research will focus on addressing these limitations by exploring adaptive and machine-learning-based controllers, conducting hardware-in-the-loop tests, and refining the grid model to ensure the robustness and practical applicability of the EHO-based optimization technique.

6. Conclusion

This study reaffirms the main theoretical contribution that EHO-based PI tuning in a STATCOM effectively maintains renewable energy system (RES) connectivity during severe grid disturbances. Simulation results illustrate that during three-phase faults, the EHO-tuned STATCOM sustains a minimum point-of-common-coupling (PCC) voltage of 0.37 p.u. (compared to 0.59 p.u. with PSO) and significantly reduces transient overshoots under wind gust conditions (2–15 m/s). These metrics underscore the value of our approach in ensuring continuous RES operation, which is critical for grid stability and reliability.

By maintaining voltage stability during faults, the proposed method helps grid operators manage large-scale intermittent sources with minimal risk of disconnection, thereby enhancing overall system reliability. EHO was selected over PSO due to its robustness to parameter variations and slightly faster convergence when navigating the nonlinear control challenges inherent in hybrid PV–WECS systems.

Looking ahead, future research will pursue the development of adaptive, machine-learning-based controllers and fuzzy-based algorithms for real-time PI gain retuning. Additionally, we plan to validate the proposed strategy through hardware-in-the-loop (HIL) tests on high-voltage grids. These directions are expected to further enhance the practicality of our approach, offering grid operators improved tools for managing dynamic and large-scale renewable integrations with reduced risk of service interruption.

Author Contribution: All authors contributed equally to the main contributor to this paper. All authors read and approved the final paper.

Funding: This research received no external funding.

Conflicts of Interest: The authors declare no conflict of interest.

Appendix

A. System Data and Parameters

1. KC200GT Module Parameters

Quantity	Value
$I_{\max power}$	7.61 A
$V_{\max power}$	26.3 V
$P_{\max}$	200.143 W
I_{sc}	8.21 A
V_{oc}	32.9 V
$I_{leakage}$	$9.825 \times 10^{-8}\,A$
$I_{photovoltaic}$	8.211 A
Diode ideality (a)	1.3
Parallel resistance	415.406 Ω
Series resistance	0.221 Ω

2. SRG Parameters

$\alpha = 1°$

$\beta = 16$

$V_o = 230\,V$

$I_{dc} = 99.2\,A$

$P_{out} = 24.8\,kW$

3. STATCOM Data

Rating	48 kVA
Line resistance	0.34 Ω
Line reactance	3.63 Ω
DC-link capacitance	250 μF

B. STATCOM Modeling

The general mathematical model of the STATCOM can be expressed in terms of active power (P), reactive power (Q), and STATCOM output voltage ($V_{STATCOM}$):

$$P = \frac{V_{bus} \times V_{STATCOM}}{X_L} \sin(\alpha) \tag{1}$$

$$Q = \frac{V_{bus} \times V_{bus}}{X_L} - \frac{V_{bus} \times V_{STATCOM}}{X_L} \cos(\alpha) \tag{2}$$

On the AC side, the first-order differential equations are:

$$\frac{dI_{sa}}{dt} = \frac{1}{L_s}(-R_s I_{sa} + E_{sa} - E_{ta}), \tag{3}$$

$$\frac{dI_{sb}}{dt} = \frac{1}{L_s}(-R_s I_{sb} + E_{sb} - E_{tb}), \tag{4}$$

$$\frac{dI_{sc}}{dt} = \frac{1}{L_s}(-R_s I_{sc} + E_{sc} - E_{tc}). \tag{5}$$

When converted into the rotating (R–I) reference frame:

$$I_{sR} I_{sI} = -R_s L_s w_0 \quad \cdots \tag{6}$$

On the DC side, the voltage is governed by:

$$\frac{dV_{dc}}{dt} = \frac{1}{C_s}(I_{dc} + V_{dc}) \tag{7}$$

Ensuring power balance:

$$V_{dc}\, I_{dc} = \frac{3}{2}(E_{sR}\, I_{sR} + E_{sI}\, I_{tI}) \tag{8}$$

C. Elephant Herding Optimization Equations

Equations (9)-(12) detail how elephant positions are updated in EHO. In the main text (Section 3.6), you can reference "Appendix, Section C" for these derivations.

$$x'_{i,j} = x_{i,j} + \alpha\left(x_{\text{best},j} - x_{i,j}\right) r \tag{9}$$

$$x_{\text{best},j} = \beta\, x_{\text{center},j} \tag{10}$$

$$x_{\text{center},j} = \frac{1}{N}\sum_{i=1}^{N} x_{i,j} \tag{11}$$

$$x_{\text{worst},j} = x(\{xmin, xmax\}_{\text{min}}) \tag{12}$$

Where:

$x_{i,j}$ is the ith elephant's position in the jth clan,

α is a scaling factor in [0,1],

r is a uniform random variable in [0,1],

β is the matriarch's scaling factor in [0,1],

$x_{\text{center},j}$ is the average position of the jth clan, and

$x_{\text{worst},j}$ denotes the worst-positioned elephant for additional exploration.

References

[1] W. S. Hassanein, M. M. Ahmed, M. O. A. El-Raouf, M. G. Ashmawy, and M. I. Mosaad, "Performance improvement of off-grid hybrid renewable energy system using dynamic voltage restorer," *Alexandria Engineering Journal*, vol. 59, no. 3, pp. 1567–1581, 2020, https://doi.org/10.1016/j.aej.2020.03.037.

[2] G. S. Chawda *et al.*, "Comprehensive Review on Detection and Classification of Power Quality Disturbances in Utility Grid With Renewable Energy Penetration," *IEEE Access*, vol. 8, pp. 146807-146830, 2020, https://doi.org/10.1109/ACCESS.2020.3014732.

[3] S. Liaquat, M. S. Fakhar, S. A. R. Kashif, A. Rasool, O. Saleem and S. Padmanaban, "Performance Analysis of APSO and Firefly Algorithm for Short Term Optimal Scheduling of Multi-Generation Hybrid Energy System," *IEEE Access*, vol. 8, pp. 177549-177569, 2020, https://doi.org/10.1109/ACCESS.2020.3027436.

[4] M. O. A. El-Raouf, M. Aljohani, M. I. Mosaad, and T. A. AbdulFattah, "Mitigating misfire and fire-through faults in hybrid renewable energy systems utilizing dynamic voltage restorer," *Energies*, vol. 15, no. 16, p. 5769, 2022, https://doi.org/10.3390/en15165769.

[5] H. Bahrampour, A. K. B. Marnani, M. B. Askari, and M. R. Bahrampour, "Evaluation of renewable energies production potential in the Middle East: Confronting the world's energy crisis," *Frontiers in Energy*, vol. 14, no. 1, pp. 42–56, 2020, https://doi.org/10.1007/s11708-017-0486-2.

[6] A. Niccolai, F. Grimaccia, G. D. Lorenzo, R. Araneo, F. Ughi and M. Polenghi, "A Review of Floating PV Systems With a Techno-Economic Analysis," *IEEE Journal of Photovoltaics*, vol. 14, no. 1, pp. 23-34, 2024, https://doi.org/10.1109/JPHOTOV.2023.3319601.

[7] H. Benbouhenni, N. Bizon, I. Colak, M. I. Mosaad, and M. Yessef, "Direct active and reactive powers control of double-powered asynchronous generators in multi-rotor wind power systems using modified synergetic control," *Energy Reports*, vol. 10, pp. 4286–4301, 2023, https://doi.org/10.1016/j.egyr.2023.10.085.

[8] A. A. Hafez, Y. F. Nassar, M. I. Hammdan, and S. Y. Alsadi, "Technical and economic feasibility of utility-scale solar energy conversion systems in Saudi Arabia," *Iranian Journal of Science and Technology, Transactions of Electrical Engineering*, vol. 44, no. 1, pp. 213–225, 2020, https://doi.org/10.1007/s40998-019-00233-3.

[9] H. J. El-Khozondar, F. El-Batta, R. J. El-Khozondar, Y. Nassar, M. Alramlawi, and S. Alsadi, "Standalone hybrid PV/wind/diesel-electric generator system for a COVID-19 quarantine center," *Environmental Progress & Sustainable Energy*, vol. 42, no. 3, p. e14049, 2023, https://doi.org/10.1002/ep.14049.

[10] Y. F. Nassar *et al.*, "Carbon footprint and energy life cycle assessment of wind energy industry in Libya," *Energy Conversion and Management*, vol. 300, p. 117846, 2024, https://doi.org/10.1016/j.enconman.2023.117846.

[11] N. G. Hingorani, "High power electronics and flexible AC transmission system," *IEEE Power Engineering Review*, vol. 8, no. 7, pp. 3–4, 1988, https://doi.org/10.1109/MPER.1988.590799.

[12] M. I. Mosaad, M. O. A. El-Raouf, M. A. Al-Ahmar, and F. M. Bendary, "Optimal PI controller of DVR to enhance the performance of hybrid power system feeding a remote area in Egypt," *Sustainable Cities and Society*, vol. 47, p. 101469, 2019, https://doi.org/10.1016/j.scs.2019.101469.

[13] R. Fadaeinedjad, G. Moschopoulos and M. Moallem, "Using STATCOM to mitigate voltage fluctuations due to aerodynamic aspects of wind turbines," *2008 IEEE Power Electronics Specialists Conference*, pp. 3648-3654, 2008, https://doi.org/10.1109/PESC.2008.4592522.

[14] M. I. Mosaad, H. S. M. Ramadan, M. Aljohani, M. F. El-Naggar and S. S. M. Ghoneim, "Near-Optimal PI Controllers of STATCOM for Efficient Hybrid Renewable Power System," *IEEE Access*, vol. 9, pp. 34119-34130, 2021, https://doi.org/10.1109/ACCESS.2021.3058081.

[15] Y. M. Alharbi, A. M. S. Yunus and A. A. Siada, "Application of UPFC to improve the LVRT capability of wind turbine generator," *2012 22nd Australasian Universities Power Engineering Conference (AUPEC)*, pp. 1-4, 2012, https://ieeexplore.ieee.org/document/6360253.

[16] H. Sebaa, K. R. Guerriche and T. Bouktir, "Optimal sizing and placement of renewable energy source in large scale power system using ABC technique in presence of UPFC," *2014 International Renewable and*

Sustainable Energy Conference (IRSEC), pp. 294-299, 2014, https://doi.org/10.1109/IRSEC.2014.7059912.

[17] E. M. Molla and C. C. Kuo, "Voltage sag enhancement of grid connected hybrid PV-wind power system using battery and SMES based dynamic voltage restorer," *IEEE Access*, vol. 8, pp. 130003–130013, 2020, https://doi.org/10.1109/ACCESS.2020.3009420.

[18] Dawei Xiang, Li Ran, P. J. Tavner and S. Yang, "Control of a doubly fed induction generator in a wind turbine during grid fault ride-through," *IEEE Transactions on Energy Conversion*, vol. 21, no. 3, pp. 652-662, 2006, https://doi.org/10.1109/TEC.2006.875783.

[19] S. Wang, S. Chen, L. Ge and L. Wu, "Distributed Generation Hosting Capacity Evaluation for Distribution Systems Considering the Robust Optimal Operation of OLTC and SVC," *IEEE Transactions on Sustainable Energy*, vol. 7, no. 3, pp. 1111-1123, 2016, https://doi.org/10.1109/TSTE.2016.2529627.

[20] M. F. El-Naggar, M. I. Mosaad, H. M. Hasanien, T. A. AbdulFattah, and A. F. Bendary, "Elephant herding algorithm-based optimal PI controller for LVRT enhancement of wind energy conversion systems," *Ain Shams Engineering Journal*, vol. 12, no. 1, pp. 599–608, 2021, https://doi.org/10.1016/j.asej.2020.07.013.

[21] H. Kuang, L. Zheng, S. Li, and X. Ding, "Voltage stability improvement of wind power grid-connected system using TCSC-STATCOM control," *IET Renewable Power Generation*, vol. 13, no. 2, pp. 215–219, 2019, https://doi.org/10.1049/iet-rpg.2018.5492.

[22] M. I. Mosaad, "Model reference adaptive control of STATCOM for grid integration of wind energy systems," *IET Electric Power Applications*, vol. 12, no. 5, pp. 605–613, 2018, https://doi.org/10.1049/iet-epa.2017.0662.

[23] M. I. Mosaad, A. Alenany, and A. Abu-Siada, "Enhancing the performance of wind energy conversion systems using unified power flow controller," *IET Generation, Transmission & Distribution*, vol. 14, no. 10, pp. 1922–1929, 2020, https://doi.org/10.1049/iet-gtd.2019.1112.

[24] H. S. Ramadan, S. Padmanaban, and M. I. Mosaad, "Metaheuristic-based near-optimal fractional order PI controller for on-grid fuel cell dynamic performance enhancement," *Electric Power Systems Research*, vol. 208, p. 107897, 2022, https://doi.org/10.1016/j.epsr.2022.107897.

[25] R. Chedid and S. Rahman, "Unit sizing and control of hybrid wind-solar power systems," *IEEE Transactions on Energy Conversion*, vol. 12, no. 1, pp. 79-85, 1997, https://doi.org/10.1109/60.577284.

[26] D. C. Meena and A. Devanshu, "Genetic algorithm tuned PID controller for process control," *2017 International Conference on Inventive Systems and Control (ICISC)*, pp. 1-6, 2017, https://doi.org/10.1109/ICISC.2017.8068639.

[27] M. I. Mosaad, "Direct power control of SRG-based WECSs using optimised fractional-order PI controller," *IET Electric Power Applications*, vol. 14, no. 3, pp. 409–417, 2020, https://doi.org/10.1049/iet-epa.2019.0194.

[28] H. Chojaa *et al*., "A Novel DPC Approach for DFIG-Based Variable Speed Wind Power Systems Using DSpace," *IEEE Access*, vol. 11, pp. 9493-9510, 2023, https://doi.org/10.1109/ACCESS.2023.3237511.

[29] A. D. Falehi and M. Rafiee, "LVRT/HVRT capability enhancement of DFIG wind turbine using optimal design and control of novel PIλDμ-AMLI based DVR," *Sustainable Energy, Grids and Networks*, vol. 16, pp. 111–125, 2018, https://doi.org/10.1016/j.segan.2018.06.001.

[30] M. G. Villalva, J. R. Gazoli, and E. R. Filho, "Modeling and circuit-based simulation of photovoltaic arrays," *Eletrônica de Potência*, vol. 14, no. 1, pp. 35–45, 2009, https://doi.org/10.18618/REP.2009.1.035045.

[31] M. O. a. El-Raouf, M. I. Mosaad, A. Mallawany, M. A. Al-Ahmar and F. M. E. Bendary, "MPPT of PV-Wind-Fuel Cell of Off-Grid Hybrid System for a New Community," *2018 Twentieth International Middle East Power Systems Conference (MEPCON)*, pp. 480-487, 2018, https://doi.org/10.1109/MEPCON.2018.8635165.

[32] H. Chen, J. Li and X. Zhou, "PSO-based self-tuning PI control for STATCOM," *Proceedings of The 7th International Power Electronics and Motion Control Conference*, pp. 2710-2715, 2012, https://doi.org/10.1109/IPEMC.2012.6259291.

[33] B. Singh, S. S. Murthy and S. Gupta, "Analysis and design of STATCOM-based voltage regulator for self-excited induction generators," *IEEE Transactions on Energy Conversion*, vol. 19, no. 4, pp. 783-790, 2004, https://doi.org/10.1109/TEC.2004.827710.

[34] F. Z. Peng and Jin Wang, "A universal STATCOM with delta-connected cascade multilevel inverter," *2004 IEEE 35th Annual Power Electronics Specialists Conference (IEEE Cat. No.04CH37551)*, vol. 5, pp. 3529-3533, 2004, https://doi.org/10.1109/PESC.2004.1355099.

[35] N. K. Saxena and A. Kumar, "Reactive power control in decentralized hybrid power system with STATCOM using GA, ANN and ANFIS methods," *International Journal of Electrical Power & Energy Systems*, vol. 83, pp. 175-187, 2016, https://doi.org/10.1016/j.ijepes.2016.04.009.

[36] N. K. Saxena and A. Kumar, "Reactive power compensation of an isolated hybrid power system with load interaction using ANFIS tuned STATCOM," *Frontiers in Energy*, vol. 8, no. 2, pp. 261–268, 2014, https://doi.org/10.1007/s11708-014-0298-6.

[37] P. R. Sahu, P. K. Hota, and S. Panda, "Modified whale optimization algorithm for fractional-order multi-input SSSC-based controller design," *Optimal control applications and methods*, vol. 39, no. 5, pp. 1802-1817, 2018, https://doi.org/10.1002/oca.2443.

[38] H. Le-Huy, "Performance study of a four-phase 8/6 switched reluctance generator using a nonlinear model based on magnetization curves," *2009 35th Annual Conference of IEEE Industrial Electronics*, pp. 3910-3915, 2009, https://doi.org/10.1109/IECON.2009.5415348.

[39] N. F. Ibrahim *et al*., "A new adaptive MPPT technique using an improved INC algorithm supported by fuzzy self-tuning controller for a grid-linked photovoltaic system," *PLoS One*, vol. 18, no. 11, p. e0293613, 2023, https://doi.org/10.1371/journal.pone.0293613.

[40] A. Ouannou *et al*., "Parameter identification of switched reluctance motor SRM using exponential swept-sine signal," *Machines*, vol. 11, no. 6, p. 625, 2023, https://doi.org/10.3390/machines11060625.

[41] O. M. Lamine, N. Bessous, B. Abdelhalim, F. A. Banakhr, M. I. Mosaad, M. Oussama, and M. M. Mahmoud, "A Combination of INC and Fuzzy Logic-Based Variable Step Size for Enhancing MPPT of PV Systems," *International Journal of Robotics and Control Systems*, vol. 4, no. 2, pp. 877–892, 2024, https://doi.org/10.31763/ijrcs.v4i2.1428.

[42] G. -G. Wang, S. Deb and L. d. S. Coelho, "Elephant Herding Optimization," *2015 3rd International Symposium on Computational and Business Intelligence (ISCBI)*, pp. 1-5, 2015, https://doi.org/10.1109/ISCBI.2015.8.

[43] M. S. Alam, F. S. Al-Ismail, and M. A. Abido, "PV/wind-integrated low-inertia system frequency control: PSO-optimized fractional-order PI-based SMES approach," *Sustainability*, vol. 13, no. 14, p. 7622, 2021, https://doi.org/10.3390/su13147622.

[44] M. I. Mosaad, "Adaptive control universality of STATCOM for efficient wind energy conversion systems," *Wind Engineering*, 2024, https://doi.org/10.1177/0309524X241266947.

[45] R. B. Bollipo, S. Mikkili, and P. K. Bonthagorla, "Hybrid, optimal, intelligent and classical PV MPPT techniques: A review," *CSEE Journal of Power and Energy Systems*, vol. 7, no. 1, pp. 9–33, 2021, https://doi.org/10.17775/CSEEJPES.2019.02720.

[46] J. Li, H. Lei, A. H. Alavi, and G.-G. Wang, "Elephant Herding Optimization: Variants, Hybrids, and Applications," *Mathematics*, vol. 8, no. 9, p. 1415, 2020, https://doi.org/10.3390/math8091415.

[47] F. Chakraborty, P. K. Roy, and D. Nandi, "Oppositional elephant herding optimization with dynamic cauchy mutation for multilevel image thresholding," *Evolutionary Intelligence*, vol. 12, pp. 445–467, 2019, https://doi.org/10.1007/s12065-019-00238-1.

[48] K. U. Chowdary and B. Prabhakara Rao, "Performance improvement in MIMO-OFDM systems based on adaptive whale elephant herd optimization algorithm," *International Journal of Engineering and Advanced Technology*, vol. 9, pp. 6651–6657, 2019, https://doi.org/10.35940/ijeat.A1916.109119.

[49] M. A. Elhosseini, R. A. El Sehiemy, Y. I. Rashwan, and X. Z. Gao, "On the performance improvement of elephant herding optimization algorithm," *Knowledge-Based Systems*, vol. 166, pp. 58–70, 2019, https://doi.org/10.1016/j.knosys.2018.12.012.

[50] I. A. ElShaarawy, E. H. Houssein, F. H. Ismail, and A. E. Hassanien, "An exploration-enhanced elephant herding optimization," *Engineering Computations*, vol. 36, no. 9, pp. 3029–3046, 2019, https://doi.org/10.1108/EC-09-2018-0424.